

CodeBrain: Imputing Any Brain MRI via Modality- and Instance-Specific Codes

Yicheng Wu¹(✉), Tao Song², Zhonghua Wu³, Jin Ye¹, Zongyuan Ge¹, Zhaolin Chen¹, and Jianfei Cai¹
¹Monash University, Clayton, Australia
²Fudan University, Shanghai, China
³Nanyang Technological University, Singapore, Singapore

Abstract

Unified MRI imputation, which can adapt to diverse imputation scenarios, is highly desirable as it reduces scanning costs and provides comprehensive MRI information for improved clinical diagnosis. Existing unified MRI imputation methods either rely on specific prompts to guide their transformation network or require multiple modality-specific modules. However, these approaches struggle to capture large modality and instance variations or become too complex to generalize effectively. To address these limitations, we propose **CodeBrain**, a fundamentally different pipeline for unified brain MRI imputation. **Our key idea** is to reframe various inter-modality transformations as a full-modality code prediction task via a two-stage framework. In the first stage, CodeBrain reconstructs a target modality from any other modalities by learning a compact scalar-quantized code for each instance and modality. Any target modality can then be reconstructed with high fidelity by combining the corresponding code with shared features extracted from any available modality. In the second stage, a projection encoder is trained to predict full-modality compact codes from any incomplete MRI samples, effectively simulating various imputation scenarios. We evaluate our CodeBrain on two public brain MRI datasets (i.e., IXI and BraTS 2023). Extensive experiments demonstrate that CodeBrain outperforms state-of-the-art methods, setting a new benchmark for unified brain MRI imputation. Our code will be released.

1. Introduction

Magnetic resonance imaging (MRI) is widely utilized in clinical practice due to its non-invasive capacity to distinguish between various tissue types, providing essential information for medical diagnosis and understanding brain

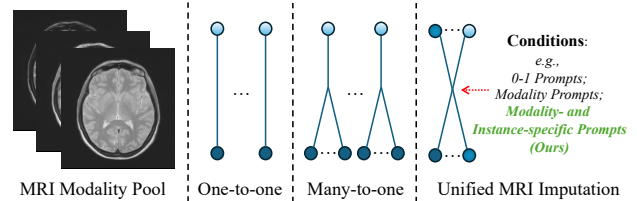


Figure 1. Illustration of different MRI imputation settings. Given multiple MRI modalities, there are various *one-to-one* and *many-to-one* transformation scenarios for synthesizing a missing one. Our proposed CodeBrain model aims to achieve a unified imputation by leveraging modality- and instance-specific prompts (i.e., learnable codes) to generate any missing brain MRI modality.

development [13, 27]. It includes a range of protocols, each producing distinct modalities that highlight specific regions of interest. For instance, T1-weighted scans are commonly used to display anatomical structures, while fluid-attenuated inversion recovery (FLAIR) scanning is a popular lesion identification tool. Additionally, contrast-enhanced modalities, such as the T1-weighted images with gadolinium (T1Gd), can further enhance abnormal regions. However, collecting a complete set of MRI modalities is often impractical since full-modality MRI screenings are both time-consuming and costly, and the use of contrast agents may lead to potential health risks [14, 44]. Furthermore, artifacts, often arising from motion, are typically unavoidable in clinical settings, resulting in subject-level registration errors [1]. These limitations motivate the development of AI models to impute missing MRI modalities to improve clinical accessibility and diagnostic completeness.

Deep learning-based imputation models [11] have made great progress in recent years, hypothesizing that *different imaging modalities for a given subject should have similar and transformable information*. This assumption is widely supported in the medical domain [35]. For instance, pancreatic cancers can be segmented from non-contrast CT images even when they are undetectable to human experts [4]. Similarly, SynthStrip [19] and SynthSeg [2] achieve

Correspondence to yicheng.wu@monash.edu. Yicheng Wu and Tao Song contributed equally to this work.

robust anatomical structure segmentation across different brain modalities, further suggesting the structural similarity among different modalities. Consequently, restoring missing information from limited modalities in brain MRI is feasible. As illustrated in Fig. 1, prior approaches mainly focus on various *One-to-one* or *Many-to-one* synthesis scenarios, aiming to generate the desired target from a single or a set of available data. To improve synthesis performance, various techniques have been explored, including generative adversarial networks (GANs) [10, 39], diffusion models [24, 30], and transformer architectures [8, 29]. However, imputation scenarios can vary widely. For example, with four common MRI modalities (*e.g.*, T1, T2, FLAIR, and T1Gd), up to 12 one-to-one models are required to cover all possible imputation requirements. As a result, developing a unified method (*i.e.*, *N-to-N* synthesis) that can adapt to different MRI imputation scenarios is highly desirable, which can streamline clinical deployment and achieve large-scale model training by leveraging all available data.

Existing unified methods typically rely on conditional prompts to specify task targets [25, 27, 46], *e.g.*, using binary codes to denote different imputation task settings [30]. Additionally, trainable prompts can be learned to represent various modalities [29]. However, approaches that employ either binary or modality-specific prompts within a single transformation network struggle to capture the extensive modality and instance variations, *i.e.*, the intricate differences in style and structure across individual samples. To address this challenge, some methods [29, 51] introduce multiple modality-specific modules. However, this design increases architectural complexity and computational demands, making it difficult to generalize and scale.

The limitations of existing unified imputation approaches motivate us to propose *CodeBrain*, a fundamentally different pipeline for unified brain MRI imputation. **Our key idea** is to simplify the complex *N-to-N* synthesis task using a *divide-and-conquer* strategy. Specifically, we design a two-stage framework. The first stage constructs a latent space by disentangling each instance’s latent features into modality-agnostic and modality-specific features. This separation ensures that modality-agnostic information—extractable from any available modalities—is handled independently, while the second stage focuses solely on completing the missing modality-specific information.

To further simplify the synthesis task in the second stage, we encode modality- and instance-specific features as low-dimensional scalar-quantized codes. In other words, the first stage reconstructs a target modality from a source modality, learning a compact scalar-quantized code for each instance and modality. Any target modality can then be reconstructed at high quality by combining the corresponding code with shared features extracted from any available subject-level modality. With this finite discrete code space,

the second stage trains a projection encoder to predict full-modality codes from any incomplete MRI samples, effectively simulating different imputation scenarios.

Our major contributions can be summarized as follows.

- We introduce a novel paradigm for unified brain MRI imputation based on modality- and instance-specific low-dimensional quantized codes. This approach effectively captures instance-level characteristics and transforms the complex unified modality transformation task into a more manageable full-modality code prediction task.
- We design CodeBrain as a two-stage training framework. The first stage extracts modality-agnostic features and learns modality- and instance-specific quantized codes through a reconstruction process. The second stage predicts full-modality codes using a customized grading loss.
- Extensive experiments on two datasets demonstrate that CodeBrain outperforms four state-of-the-art (SOTA) methods, achieving superior imputation quality and setting a new benchmark for unified brain MRI imputation. Meanwhile, the CodeBrain-imputed modalities can further facilitate brain tumor segmentation on BraTS 2023.

2. Related Work

MRI Imputation. Data incompleteness is a prevalent challenge in various medical AI applications. Considering the limited accessibility of comprehensive medical data, deep learning models have been applied to generate various missing targets [3, 11, 16, 33]. For example, [34] proposed a 3D cycle-GAN model to generate the corresponding PET from MRI to aid in Alzheimer’s disease diagnosis. An image-to-image translation model was developed in [44] to synthesize the cerebral blood volume data from standard MRI modalities, enhancing its clinical applicability.

Recent studies have focused on unified MRI imputation. For instance, MMSYN [6] proposed to learn a modality-invariant latent representation that can be decoded into different MRI modalities. MMGAN [39] employed GAN models to improve the synthesis quality. MMT [29] utilized a Swin Transformer with modality-dependent queries to generate missing modalities. M2DN [30] applied a diffusion model with binary conditional codes to specify different imputation tasks. Furthermore, [51] explored the use of modality-shared and modality-specific modules to improve unified imputation performance, and [9] incorporated federated learning for multi-modal MRI synthesis.

Nevertheless, most existing unified approaches still operate in a pixel-to-pixel inter-modality transformation scheme. In contrast, our proposed CodeBrain framework performs inter-modality transformation at the quantized latent code level and synthesizes a missing modality with the predicted code plus the extracted common features, which achieves a more robust mapping across modalities and eliminates the need for modality-specific modules.

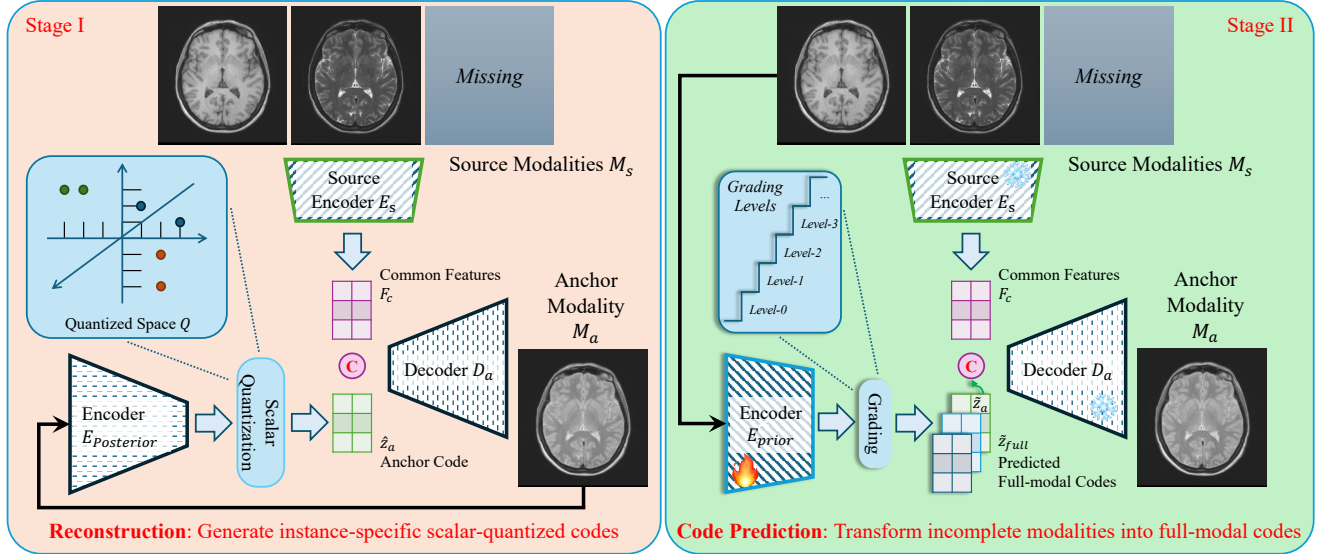


Figure 2. **Pipeline of our proposed CodeBrain framework for unified Brain MRI imputation.** It consists of two training stages: Stage I constructs a latent quantized space, where any target anchor is projected to its particular scalar code by $E_{posterior}$ and then reconstructed by D_a using this code along with the common features F_c extracted from any input incomplete modalities by E_s . Stage II aims to predict full-modality scalar-quantized codes from any available source modalities by E_{prior} with a grading loss. During inference, the decoder D_a synthesizes the missing anchor modality using the predicted anchor code by E_{prior} and the extracted common features from input incomplete modalities via E_s . Note that all modules here are modality-agnostic.

Quantization-based Image Generation. Quantization projects complex data into a low-dimensional representation, facilitating multi-modal alignment, mapping, and fusion [18]. Data-driven vector quantization (VQ) techniques have been widely applied in image-based reconstruction, transformation, and generation tasks [12]. Solutions like the straight-through estimator (STE) [43] and Gumbel-softmax [22] are commonly used to back-propagate gradients in quantization modules, enabling end-to-end training. For example, VQVAE [43] introduced the neural discrete representation, while VQGAN [12] employed a patch GAN model to capture fine details and a transformer to predict code indices for high-resolution image synthesis. To improve the image generation quality, residual designs [28], multi-scale codebooks [37, 45], dynamic token embeddings [20], code splitting [53] have been proposed to improve VQ representation capacity. Recently, beyond region-level VQ, global quantization methods [41, 49] have been explored to disentangle multi-level visual signals. Furthermore, VQ has been incorporated with the diffusion and transformer models [15, 38, 40] to produce high-fidelity generation results.

However, training a robust codebook with high utilization is still a critical challenge in VQ-related studies [31]. Therefore, implicit codebooks have been introduced, where the decoder reconstructs targets from only code indices instead of relying on the nearest learnable code vectors [17]. For example, MAGVIT [48] introduced lookup-free quanti-

zation [5] by compressing data into binary indices, achieving superior video generation results. FSQ [31] proposed to use scalar quantization with a straightforward rounding operation, discarding the complex process of learning an effective codebook. Following them, our proposed CodeBrain model generates scalar-quantized codes in a finite discrete space, which can be seen as modality- and instance-specific prompts followed by the enhancement of common features to improve brain MRI reconstruction performance.

3. Method

Fig. 2 provides an overview of our proposed CodeBrain model. The core idea is to perform inter-modality transformations as predicting scalar-quantized codes in a latent quantized space Q while recovering any missing modality by decoding its recovered code with the extracted common features from any available modality. Specifically, the training process consists of two stages. Stage I constructs a finite scalar space and quantizes each sample into a specific code map. Then, Stage II predicts full-modality codes from any incomplete MRI inputs, supervised by corresponding codes constructed in Stage I, to achieve a unified brain MRI imputation. During inference, given incomplete input, we use the prior encoder E_{prior} to predict the scalar-quantized codes for any missing modality and feed them, together with the common features extracted by the encoder E_s , to the decoder D_a to recover the missing modality.

3.1. Stage I: Reconstruction

The purpose of Stage I is to reconstruct an anchor modality M_a from incomplete source modalities M_s ($M_s \neq M_a$) via an encoder (E_s) and decoder (E_a) architecture. The uniqueness of our Stage I is the design of the **bottleneck feature representation**, which consists of a common feature extracted from M_s by E_s and an anchor code extracted from M_a by a posterior encoder $E_{posterior}$, aiming to capture modality-agnostic information and anchor-specific information, respectively.

Specifically, given a subject containing N distinct MRI modalities, M_s is a concatenation along the channel dimension of different modalities. We then perform random masking to simulate various imputation scenarios. Specifically, we randomly mask k channels out of N channels/modalities, with $0 < k < N$. Then, we randomly select a missing one as the anchor M_a . Following [31], we first encode M_a into a low-dimensional latent feature F_a of size $d \times h \times w$ by $E_{posterior}$, and then element-wise scalar-quantize it to L values as

$$\begin{aligned} F_a &= E_{posterior}(M_a) \\ Z_a &= \lfloor L/2 \rfloor \times \tanh(F_a) \\ \hat{Z}_a &= \text{Round}(Z_a), \end{aligned} \quad (1)$$

where $Z_a \in d \times h \times w$ is the bounded feature and \hat{Z}_a is the scalar-quantized anchor code via rounding. To enable end-to-end training, following STE [43], \hat{Z}_a can be represented as $(Z_a + sg[\hat{Z}_a - Z_a])$, where $sg[\cdot]$ is the stop-gradient operation, essentially copying the gradients before and after Round . Note that, Z_a has d dimensions and the scalar quantization is performed at each dimension. There are L possible integer values for each dimension, and the total possible number of quantized vectors (*i.e.*, codes) is L^d . Additionally, each element in \hat{Z}_a indicates a quantized representation for an image patch in M_a . Such a simple scalar quantization introduced in [31] does not require learning an explicit codebook with no auxiliary losses [47] needed to regularize the training.

Since the quantization process is lossy and the code is low-dimensional, it cannot restore all details of anchor M_a . To improve the synthesis quality, we exploit a source encoder E_s to generate common features F_c from M_s . Note that, F_c is modality-agnostic, which is achieved by extracting F_c from any incomplete modality and enforcing it to contribute to any other modality. Specifically, we have

$$\begin{aligned} F_c &= E_s(M_s), \\ \tilde{M}_a &= D_a(\text{Concat}[\hat{Z}_a, F_c]) \end{aligned} \quad (2)$$

where \tilde{M}_a denotes the corresponding reconstructed results from D_a with the concatenated input of both \hat{Z}_a and F_c . Finally, we train the Stage I model with the following overall

reconstruction loss:

$$\mathcal{L}_{rec} = \mathcal{L}_{psnr}(\tilde{M}_a, M_a) + \lambda \times \mathcal{L}_{gan}(\tilde{M}_a, M_a) \quad (3)$$

where \mathcal{L}_{psnr} is a differentiable loss of Peak Signal-to-Noise Ratio (PSNR) [7], \mathcal{L}_{gan} is a PatchGAN loss [21] to capture the image details, and λ is a hyper-parameter to balance the two terms during training.

Our Stage I designs have several advantages: 1) Different modalities are projected to a shared low-dimensional quantized latent space, reducing the inter-modality gap; 2) \hat{Z}_a is modality- and instance-specific, while F_c aims to capture the modality-shared information, bridging both Stage I and Stage II; 3) The model training only relies on two losses, avoiding the complex tuning of many optimization targets.

3.2. Stage II: Code Prediction

Once Stage I learns modality- and instance-specific codes in the quantized space, the purpose of Stage II is to establish inter-modality transformation by directly predicting the scalar codes of missing modalities.

Specifically, a prior encoder E_{prior} is trained to generate full-modality codes \tilde{Z}_{full} from the incomplete input M_s , supervised by \hat{Z}_{full} , a channel-wise concatenation of quantized codes of N MRI modalities from Stage I:

$$\begin{aligned} \tilde{Z}_{full} &= E_{prior}(M_s) \\ \mathcal{L}_{pred} &= \mathcal{D}(\tilde{Z}_{full}, \hat{Z}_{full}) \end{aligned} \quad (4)$$

where \mathcal{D} measures the distance between \tilde{Z}_{full} and \hat{Z}_{full} . The target here is to predict full-modality codes so that the model is trained by the imputation of missing modalities and the reconstruction of available ones at the same time, similar to [30].

Since each code dimension can only be one of the L integers, we can directly set \mathcal{D} as a L -class cross-entropy loss to train the Stage II model. However, this design ignores the clustering characteristic of the quantized space and the distances among the pre-defined L classes [52]. Therefore, we design a grading loss for \mathcal{D} , which is defined as an ordinal binary cross-entropy loss:

$$\begin{aligned} \mathcal{L}_{pred} &= \mathcal{L}_{bce}(\tilde{B}_{full}, \hat{B}_{full}) \\ \text{s.t.}, \tilde{B}_{full} &= T(\tilde{Z}_{full}, L), \hat{B}_{full} = T(\hat{Z}_{full}, L) \end{aligned} \quad (5)$$

where T denotes a transformation from an integer value to an array of binary values of length $(L - 1)$, indicating the ordinal relationships for the original class labels. For example, given a class label y in the range of $\{0, \dots, L - 1\}$, we create B_y as:

$$B_y^j = \begin{cases} 1 & \text{if } j < y \\ 0 & \text{else} \end{cases} \quad (6)$$

where $j, j \in \{0, \dots, L-2\}$, is the bit index of B_y . Note that both \tilde{B}_{full} and \hat{B}_{full} are of size $(L-1) \times d \times h \times w$.

The advantages of our Stage II designs can be summarized as: 1) The inter-modality transformation is designed to simply predict full-modal quantized codes; 2) A grading loss is used to represent the smooth code distribution in the latent space; 3) All modules are modality-agnostic and we don’t need to rely on any modality-specific module to facilitate training.

4. Experiments and Results

4.1. Experimental Details

Datasets. We evaluated the proposed CodeBrain model on the IXI¹ and BraTS 2023² [32] datasets. IXI contains non-skull-stripped MRI samples from 577 healthy subjects, which were scanned from three London hospitals using three different MRI machines. Each subject contains T1, T2, and Proton Density-weighted (PD) modalities. Since these modalities are not spatially-registered, we then use ANTsPy³ to register T1 and PD to T2 rigidly. Then, following [29, 30], 90 transverse brain slices are extracted from the middle of each 3D volume. We then crop these slices into a fixed size of 256×256 and randomly select 500 subjects for training, 37 for validation, and the remaining 40 for testing.

BraTS 2023 comprises multi-site multi-parametric MRI (mpMRI) scans of brain tumor patients, including T1, T2, FLAIR, and T1Gd modalities. Each sample is skull-stripped and rigid-registered. As [29, 30], we extract the middle 80 transverse slices in our experiments, which are further cropped to a fixed size of 240×240 . The training, validation, and testing sets include 500, 40, and 40 randomly selected subjects, respectively.

Implementation. We first normalized these MRI slices into a fixed intensity range of 0-1 by a min-max normalization, making the voxel intensities across different subjects and different modalities comparable, same as [51]. For both datasets, we set λ to 1, the batch size to 48, and L as 5 as suggested in [31]. d is set as 9/7 on the IXI/BraTS 2023 dataset. We adopted the NAFNet [7] as the backbone and used the Adam optimizer with an initial learning rate (LR) of $1e-3$. A cosine scheduler with a minimum LR $1e-5$ was used to tune the LR to stabilize the model training. All experiments were conducted in an identical environment for fair comparisons (Hardware: $8 \times$ NVIDIA GeForce 4090 GPUs; Software: PyTorch: 2.1.2, CUDA: 11.8, Random Seed: 1234). We trained the CodeBrain model for 250 epochs in each stage. On the IXI dataset, the total computational complexity of our CodeBrain model is 157.82

GMACs with 134.56 M parameters. The total training time is around 84 hours.

Evaluation Metrics. We use three metrics to evaluate the performance: PSNR, Structural Similarity Index (SSIM), and Mean Absolute Error (MAE). Since the MRI data has a large range of voxel intensities, we use the float type rather than the 8-bit one to calculate these metrics. The data range of PSNR is fixed to 0-1. We compare our CodeBrain with two public unified models: MMSYN [6] and MMGAN [39], and two recent methods: transformer-based MMT [29] and diffusion-based M2DN [30], where the latter two were implemented according to their works. We will release our experimental settings to establish a public benchmark for unified brain MRI imputation.

4.2. Imputed Results in Different Scenarios

Table 1 gives quantitative synthesis results in different imputation scenarios on the IXI dataset. It reveals that, PD is relatively easier to synthesize from other modalities, and T2 contains more hard-to-restore details, indicating the importance of T2 examinations in clinical practice. Furthermore, different one-to-one (*i.e.*, “O→O”) imputation results (*i.e.*, the top part of Table 1) show that T1 can be better transformed from PD than T2, while T2 and PD are highly related, as stated in [27, 29]. Then, many-to-one (*i.e.* “M→O”) settings can achieve better performance in both Stage I-Reconstruction and Stage II-Imputation.

Fig. 3 further shows visualized results in different scenarios. We can see that our proposed CodeBrain model generates accurate and plausible anatomic structures for different missing modalities in different scenarios for brain MRI.

4.3. Comparisons

Table 2 gives the comparison results of our model and four existing models [6, 29, 30, 39] for unified brain MRI imputation on the IXI (Top) and BraTS 2023 (Bottom) datasets. It reveals that the CodeBrain model significantly outperforms other methods for various “O→O” and “M→O” settings on both datasets. For example, on the IXI dataset, our CodeBrain outperforms the second-best work [29] by 0.89 dB in PSNR. Furthermore, although our CodeBrain model training only adopts PSNR-related losses without applying any structural loss for supervision, it surprisingly achieves an average 0.9% gain in SSIM than [29]. This indicates that CodeBrain can achieve invariant anatomical representation among different modalities [26].

Table 2 (Bottom) further shows that our model outperforms all other methods by all metrics on the BraTS 2023 dataset. Even with inconsistent regions (*e.g.*, with or without clear tumor boundaries), our model achieves the best performance, especially in SSIM. This is critical in clinical deployments to maintain a high structural consistency among different brain MRI modalities. Fig. 4 provides vi-

¹<https://brain-development.org/ixi-dataset/>

²<https://www.synapse.org/Synapse:syn53708126/wiki/626320>

³<https://github.com/ANTsX/ANTsPy>

Table 1. Quantitative results of our CodeBrain model in different brain MRI imputation scenarios on the IXI dataset. Performance is shown as “**Stage II-Imputation (Stage I-Reconstruction)**”. Here, input incomplete modalities generate both common features (from Stage I) and modality- and instance-specific scalar-quantized codes (from Stage II) for the target modality synthesis.

Scenarios			T1			T2			PD		
T1	T2	PD	PSNR (dB) \uparrow	SSIM (%) \uparrow	MAE ($\times 1000$) \downarrow	PSNR (dB) \uparrow	SSIM (%) \uparrow	MAE ($\times 1000$) \downarrow	PSNR (dB) \uparrow	SSIM (%) \uparrow	MAE ($\times 1000$) \downarrow
		✓	28.33 (38.29)	93.38 (98.52)	18.11 (6.19)	30.19 (34.81)	93.82 (96.12)	15.73 (10.11)		N/A	
	✓		27.95 (38.25)	93.12 (98.50)	19.02 (6.21)		N/A		33.63 (39.03)	96.17 (98.00)	11.29 (6.41)
✓				N/A		23.51 (30.64)	86.17 (94.23)	30.68 (14.90)	27.08 (34.82)	89.90 (96.54)	21.28 (9.46)
✓	✓			N/A			N/A		34.52 (39.27)	96.47 (98.07)	10.27 (6.26)
✓		✓		N/A		30.97 (35.08)	94.17 (96.21)	14.84 (9.90)		N/A	
	✓	✓	28.71 (38.52)	93.90 (98.59)	17.27 (6.04)		N/A			N/A	
<i>mean</i>			28.33 (38.35)	93.47 (98.54)	18.13 (6.15)	28.23 (33.51)	91.39 (95.52)	20.42 (11.64)	31.74 (37.71)	94.18 (97.54)	14.28 (7.38)

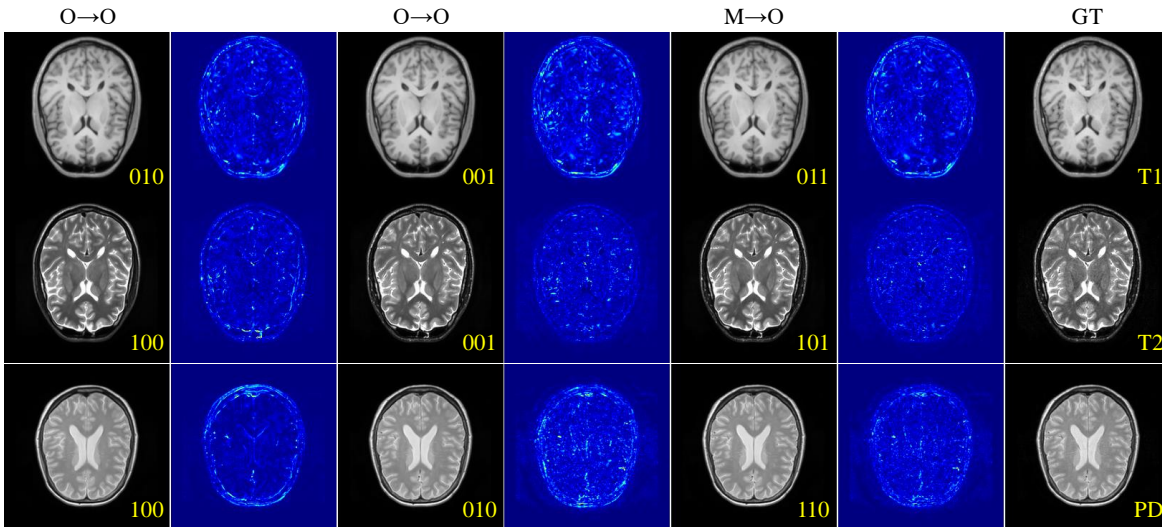


Figure 3. Exemplar synthesized brain MRI scans of our CodeBrain on the IXI dataset. 1st and 3rd columns: O→O imputed results; 5th column: M→O imputed results; 7th column: the original modality; Each synthesized scan is equipped with its corresponding error map on the right. The three bits in an annotation “010” correspond to T1, T2, and PD, respectively, where “1” indicates that modality is available.

sual comparison results in the “T2→T1” and “T1, PD→T2” scenarios on the IXI dataset. It can be seen that our model has fewer synthesis errors than other methods (*e.g.*, the brain tissues).

4.4. Ablation Studies and Discussions

Effects of Common Features. The common features F_c are designed to capture modality-agnostic information that can be directly extracted from any incomplete input. This allows the second stage to concentrate solely on completing modality-specific details, *i.e.*, scalar-quantized codes. As shown in Fig. 5, incorporating F_c significantly enhances the reconstruction performance in Stage I on the IXI dataset.

Effects of Grading. The grading loss (5) enforces the smoothness characteristic of the quantized space Q . Fig. 5 shows that this design simplifies the code prediction and consistently improves the imputation performance on IXI.

Selection of d . The code dimension d controls the com-

plexity of Q in our CodeBrain model. Fig. 5 presents results across different d on the IXI dataset. We observe that increasing d improves reconstruction performance (*e.g.*, a 1.62 dB PSNR gain from $d = 5$ to $d = 9$) while its impact on imputation performance is relatively stable (*e.g.*, a 0.11 dB PSNR gain from $d = 5$ to $d = 9$). Therefore, we select $d = 9$ as the final setting for constructing the quantized space on the IXI dataset.

Selection of Quantization. Table 3 presents an analysis of the quantization design in our CodeBrain model on the IXI dataset. In Stage I, the original VQ [12] yields inferior reconstruction performance, even with a larger codebook, which is due to the inherent difficulty of learning an explicit codebook [52]. Furthermore, when replacing our scalar-quantized codes with the continual version of the same dimension, Stage I achieves superior reconstruction performance, while the Stage II imputation performance drops. This suggests that the inter-modality transformation

Table 2. Comparison results on the IXI (Top) and BraTS 2023 (Bottom) datasets. Here, “O→O” and “M→O” indicate one-to-one and many-to-one scenarios. We can see that our proposed CodeBrain surpasses all other methods.

Metrics	MMSYN [6]			MMGAN [39]			MMT [29]			M2DN [30]			Our CodeBrain		
	O→O	M→O	ALL	O→O	M→O	ALL	O→O	M→O	ALL	O→O	M→O	ALL	O→O	M→O	ALL
PSNR (dB) ↑	25.88	28.97	26.91	26.11	29.07	27.10	27.52	30.59	28.54	26.51	29.31	27.44	28.45	31.40	29.43
SSIM (%) ↑	88.96	92.90	90.27	89.11	93.05	90.42	91.03	94.27	92.11	89.57	92.89	90.68	92.10	94.85	93.01
MAE (×1000) ↓	25.93	18.43	23.43	25.12	18.04	22.76	21.37	15.38	19.37	23.73	17.37	21.61	19.35	14.13	17.61
PSNR (dB) ↑	23.91	25.11	24.60	23.69	24.84	24.35	24.11	25.36	24.82	24.11	24.99	24.61	24.58	25.67	25.16
SSIM (%) ↑	88.75	90.38	89.69	88.03	89.88	89.09	88.78	90.62	89.83	88.78	90.66	89.85	89.27	90.77	90.09
MAE (×1000) ↓	24.81	21.34	22.83	25.02	21.90	23.24	23.79	20.48	21.90	23.79	20.98	22.22	22.59	19.87	21.13

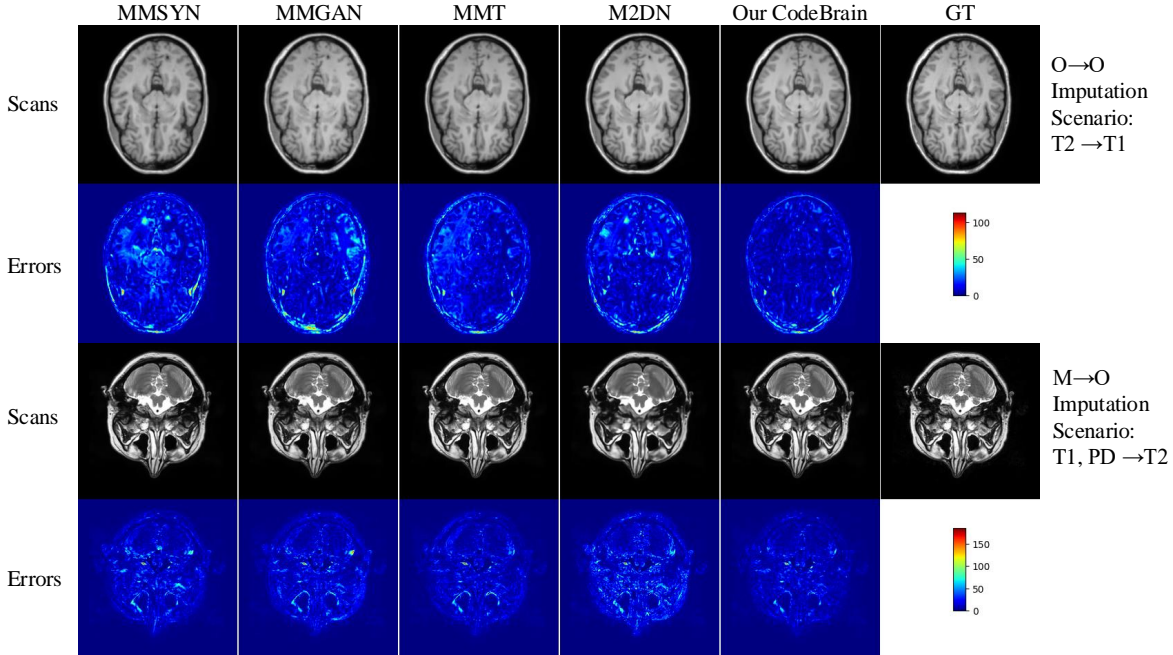


Figure 4. Exemplar comparison results between four public models and our proposed CodeBrain in the T2→T1 (Top) and T1, PD→T2 (Bottom) scenarios on the IXI dataset, along with corresponding error maps.

Table 3. Ablation studies of our CodeBrain on the IXI dataset. Here, + denotes that the VQ [12] model exploits codebook sizes of 3125/8192 with 256-dimensional code vectors for the Stage I training. * denotes using a continual latent code representation of size $9 \times 5 (d \times N)$ in our CodeBrain model.

	PSNR (dB) ↑	SSIM (%) ↑	MAE (×1000) ↓
VQ+ (Stage I-3125)	26.75	89.54	23.33
VQ+ (Stage I-8192)	26.68	89.25	23.58
Stage I (Continual)*	37.37	97.06	8.04
Stage II (Continual)*	28.55	91.77	19.17
Stage I (Discrete)	36.52	97.20	8.39
Stage II (Discrete)	29.43	93.01	17.61

becomes more challenging in the continuous latent space.

Brain Tumor Segmentation. Following [26], we perform

the inference of brain tumor segmentation, by using a U-Net model trained on real brain MRI data from BraTS 2023. Both 2D and 3D Dice scores are reported in Table 4 across four “3 → 1” imputation scenarios. The results reveal that: 1) Simply imputing missing modalities with zero values leads to a significant performance drop (see 1st row). 2) Leveraging synthesized modalities for segmentation with CodeBrain outperforms MMT [29] and M2DN [30] by a large margin. 3) CodeBrain’s imputed modalities achieve segmentation performance comparable to real brain MRI modalities (see 4th row vs. 5th row) and exhibit a strong correlation with the U-Net predictions (see 6th row). 4) Despite being trained in a 2D setting, our CodeBrain demonstrates superior 3D consistency for brain tumor segmentation on the BraTS 2023 dataset.

Quantized Codes. To visualize the distributions of quantized codes in the latent space, we further show 32×32 code

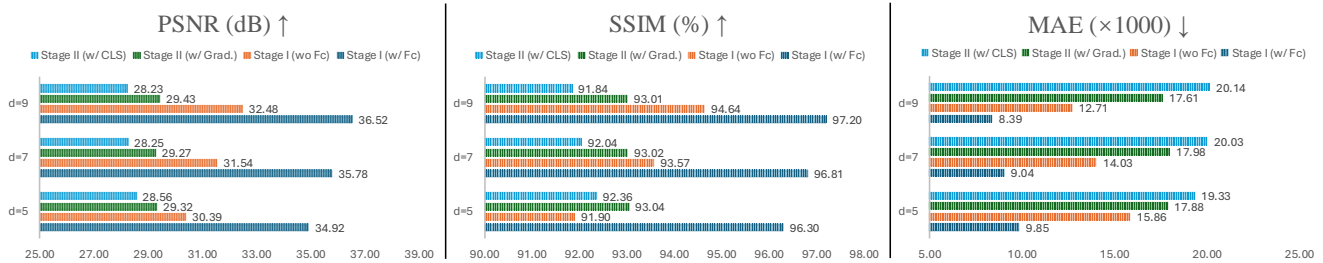


Figure 5. Ablation studies with different d in our CodeBrain on the IXI dataset. Here, common features F_c enhance the reconstruction performance, in Stage I, see “Stage I (wo F_c) vs. (w/ F_c)”, while the Stage II performance is improved by using a grading loss, see “Stage II (w/ CLS) vs. (w/ Grad.)”.

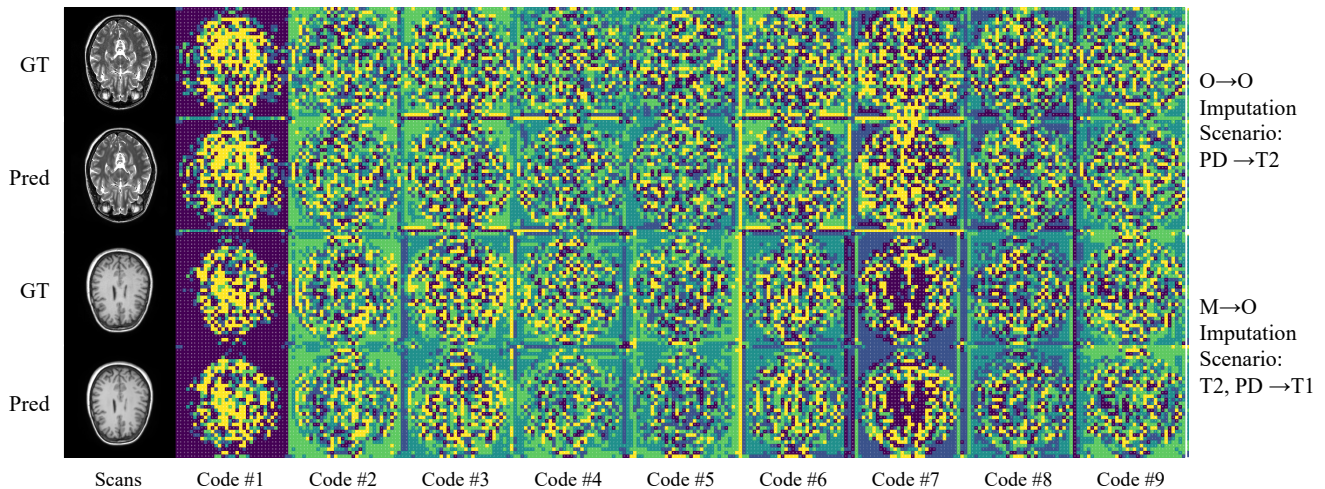


Figure 6. Exemplar 32×32 code maps of our CodeBrain on the IXI dataset. Given $d = 9$, we visualize all codes under the “PD→T2” (Top) and “T2, PD→T1” (Bottom) scenarios, showing clustered distributions in the latent quantized space Q .

Table 4. Comparisons of brain tumor segmentation in four “3 → 1” imputation scenarios, using zero imputation (1st row), synthesized imputation (2nd–4th rows), and full modalities (5th row) on BraTS 2023. Performance is reported as “2D/3D Dice (%) ↑”. Here, “CodeBrain (Seg.)” refers to the setting where the predicted segmentation results of the model trained with full modalities are used as evaluation labels.

	T1	T2	FLAIR	T1Gd
Zero Imputation	45.13/35.40	66.56/40.75	49.59/1.8	44.16/10.59
MMT [29]	76.06/71.99	82.28/76.26	80.04/73.49	61.23/27.72
M2DN [30]	82.66/75.40	84.40/76.99	83.23/76.34	68.04/48.62
CodeBrain (Ours)	86.16/80.33	85.43/78.12	85.33/77.66	70.09/43.35
Full modalities	86.31/80.45			
CodeBrain (Seg.)	95.73/93.51	95.11/92.19	92.05/89.12	75.23/48.04

maps of our CodeBrain under the “PD→T2” (Top) and “T2, PD→T1” (Bottom) scenarios in Fig. 6. We can see that, without any training regularization, the code distributions in our CodeBrain model exhibit clustering characteristics.

These clustered codes reflect coarse anatomical structures of the brain, potentially bridging image synthesis and perception tasks (*e.g.*, brain segmentation [50]). Furthermore, Stage II accurately predicts most of the corresponding codes and synthesizes high-quality brain MRI modalities on IXI.

5. Conclusion

We have presented CodeBrain, a unified model for brain MRI imputation. The key idea is to cast the unified inter-modality transformation task into two stages: reconstruction and code prediction. In the first stage, each MRI modality is compressed to a quantized code, which is augmented by common features extracted from other modalities for the reconstruction. In the second stage, CodeBrain recovers the missing codes of any incomplete MRI sample. Extensive experiments on two public datasets demonstrated the effectiveness of our CodeBrain, achieving superior performance of unified brain MRI imputation.

Limitation and Future Work. Fig. 4 shows that despite

achieving the SOTA imputation performance, our model may still be impacted by hallucination. Further improvements could come from new training losses [23, 42] and the incorporation of MRI physical theories [36], particularly for contrast-enhanced modalities such as T1Gd.

References

- [1] Guha Balakrishnan, Amy Zhao, Mert R Sabuncu, John Guttag, and Adrian V Dalca. Voxelmorph: a learning framework for deformable medical image registration. *IEEE TMI*, 38(8): 1788–1800, 2019. 1
- [2] Benjamin Billot, Douglas N Greve, Oula Puonti, Axel Thielscher, Koen Van Leemput, Bruce Fischl, Adrian V Dalca, Juan Eugenio Iglesias, et al. Synthseg: Segmentation of brain mri scans of any contrast and resolution without retraining. *Medical Image Analysis*, 86:102789, 2023. 1
- [3] Bing Cao, Zhiwei Bi, Qinghua Hu, Han Zhang, Nannan Wang, Xinbo Gao, and Dinggang Shen. Autoencoder-driven multimodal collaborative learning for medical image synthesis. *IJCV*, 131(8):1995–2014, 2023. 2
- [4] Kai Cao, Yingda Xia, Jiawen Yao, Xu Han, Lukas Lambert, Tingting Zhang, Wei Tang, Gang Jin, Hui Jiang, Xu Fang, et al. Large-scale pancreatic cancer detection via non-contrast ct and deep learning. *Nature Medicine*, 29(12): 3033–3043, 2023. 1
- [5] Huiwen Chang, Han Zhang, Lu Jiang, Ce Liu, and William T Freeman. Maskgit: Masked generative image transformer. In *CVPR*, pages 11315–11325, 2022. 3
- [6] Agisilaos Chartsias, Thomas Joyce, Mario Valerio Giuffrida, and Sotirios A Tsaftaris. Multimodal mr synthesis via modality-invariant latent representation. *IEEE TMI*, 37(3): 803–814, 2017. 2, 5, 7
- [7] Liangyu Chen, Xiaojie Chu, Xiangyu Zhang, and Jian Sun. Simple baselines for image restoration. In *ECCV*, pages 17–33, 2022. 4, 5
- [8] Onat Dalmaz, Mahmut Yurt, and Tolga Çukur. Resvit: residual vision transformers for multimodal medical image synthesis. *IEEE TMI*, 41(10):2598–2614, 2022. 2
- [9] Onat Dalmaz, Muhammad U Mirza, Gokberk Elmas, Muzaffer Ozbey, Salman UH Dar, Emir Ceyani, Kader K Oguz, Salman Avestimehr, and Tolga Çukur. One model to unite them all: Personalized federated learning of multi-contrast mri synthesis. *Medical Image Analysis*, 94:103121, 2024. 2
- [10] Salman UH Dar, Mahmut Yurt, Levent Karacan, Aykut Erdem, Erkut Erdem, and Tolga Cukur. Image synthesis in multi-contrast mri with conditional generative adversarial networks. *IEEE TMI*, 38(10):2375–2388, 2019. 2
- [11] Sanuwani Dayarathna, Kh Tohidul Islam, Sergio Uribe, Guang Yang, Munawar Hayat, and Zhaolin Chen. Deep learning based synthesis of mri, ct and pet: Review and analysis. *Medical Image Analysis*, 92:103046, 2023. 1, 2
- [12] Patrick Esser, Robin Rombach, and Bjorn Ommer. Taming transformers for high-resolution image synthesis. In *CVPR*, pages 12873–12883, 2021. 3, 6, 7
- [13] John H Gilmore, Feng Shi, Sandra L Woolson, Rebecca C Knickmeyer, Sarah J Short, Weili Lin, Hongtu Zhu, Robert M Hamer, Martin Styner, and Dinggang Shen. Longitudinal development of cortical and subcortical gray matter from birth to 2 years. *Cerebral Cortex*, 22(11):2478–2485, 2012. 1
- [14] Enhao Gong, John M Pauly, Max Wintermark, and Greg Zaharchuk. Deep learning enables reduced gadolinium dose for contrast-enhanced brain mri. *Journal of Magnetic Resonance Imaging*, 48(2):330–340, 2018. 1
- [15] Shuyang Gu, Dong Chen, Jianmin Bao, Fang Wen, Bo Zhang, Dongdong Chen, Lu Yuan, and Baining Guo. Vector quantized diffusion model for text-to-image synthesis. In *CVPR*, pages 10696–10706, 2022. 3
- [16] Alper Güngör, Salman UH Dar, Şaban Öztürk, Yılmaz Korkmaz, Hasan A Bedel, Gokberk Elmas, Muzaffer Ozbey, and Tolga Çukur. Adaptive diffusion priors for accelerated mri reconstruction. *Medical Image Analysis*, 88:102872, 2023. 2
- [17] Shaozhe Hao, Xuanton Liu, Xianbiao Qi, Shihao Zhao, Bojia Zi, Rong Xiao, Kai Han, and Kwan-Yee K Wong. Bigr: Harnessing binary latent codes for image generation and improved visual representation capabilities. *arXiv preprint arXiv:2410.14672*, 2024. 3
- [18] Dailan He, Yaoyan Zheng, Baocheng Sun, Yan Wang, and Hongwei Qin. Checkerboard context model for efficient learned image compression. In *CVPR*, pages 14771–14780, 2021. 3
- [19] Andrew Hoopes, Jocelyn S Mora, Adrian V Dalca, Bruce Fischl, and Malte Hoffmann. Synthstrip: skull-stripping for any brain image. *NeuroImage*, 260:119474, 2022. 1
- [20] Mengqi Huang, Zhendong Mao, Zhuowei Chen, and Yongdong Zhang. Towards accurate image coding: Improved autoregressive image generation with dynamic vector quantization. In *CVPR*, pages 22596–22605, 2023. 3
- [21] Phillip Isola, Jun-Yan Zhu, Tinghui Zhou, and Alexei A Efros. Image-to-image translation with conditional adversarial networks. In *CVPR*, pages 1125–1134, 2017. 4
- [22] Eric Jang, Shixiang Gu, and Ben Poole. Categorical reparameterization with gumbel-softmax. *arXiv preprint arXiv:1611.01144*, 2016. 3
- [23] Liming Jiang, Bo Dai, Wayne Wu, and Chen Change Loy. Focal frequency loss for image reconstruction and synthesis. In *ICCV*, pages 13919–13929, 2021. 9
- [24] Lan Jiang, Ye Mao, Xiangfeng Wang, Xi Chen, and Chao Li. Cola-diff: Conditional latent diffusion model for multimodal mri synthesis. In *MICCAI*, pages 398–408, 2023. 2
- [25] Simon Kohl, Bernardino Romera-Paredes, Clemens Meyer, Jeffrey De Fauw, Joseph R Ledsam, Klaus Maier-Hein, SM Eslami, Danilo Jimenez Rezende, and Olaf Ronneberger. A probabilistic u-net for segmentation of ambiguous images. In *NeurIPS*, 2018. 2
- [26] Dominic LaBella, Maruf Adewole, Michelle Alonso-Basanta, Talissa Altes, Syed Muhammad Anwar, Ujjwal Baid, Timothy Bergquist, Radhika Bhalariao, Sully Chen, Verena Chung, et al. The asnr-miccai brain tumor segmentation (brats) challenge 2023: Intracranial meningioma. *arXiv preprint arXiv:2305.07642*, 2023. 5, 7
- [27] Dongwook Lee, Won-Jin Moon, and Jong Chul Ye. Assessing the importance of magnetic resonance contrasts using

- collaborative generative adversarial networks. *Nature Machine Intelligence*, 2(1):34–42, 2020. 1, 2, 5
- [28] Doyup Lee, Chiheon Kim, Saehoon Kim, Minsu Cho, and Wook-Shin Han. Autoregressive image generation using residual quantization. In *CVPR*, pages 11523–11532, 2022. 3
- [29] Jiang Liu, Srivathsa Pasumarthi, Ben Duffy, Enhao Gong, Keshav Datta, and Greg Zaharchuk. One model to synthesize them all: Multi-contrast multi-scale transformer for missing data imputation. *IEEE TMI*, 42(9):2577–2591, 2023. 2, 5, 7, 8
- [30] Xiangxi Meng, Kaicong Sun, Jun Xu, Xuming He, and Dinggang Shen. Multi-modal modality-masked diffusion network for brain mri synthesis with random modality missing. *IEEE TMI*, 43(7):2587–2598, 2024. 2, 4, 5, 7, 8
- [31] Fabian Mentzer, David Minnen, Eirikur Agustsson, and Michael Tschannen. Finite scalar quantization: Vq-vae made simple. In *ICLR*, 2024. 3, 4, 5
- [32] Bjoern H Menze, Andras Jakab, Stefan Bauer, Jayashree Kalpathy-Cramer, Keyvan Farahani, Justin Kirby, Yuliya Burren, Nicole Porz, Johannes Slotboom, Roland Wiest, et al. The multimodal brain tumor image segmentation benchmark (brats). *IEEE TMI*, 34(10):1993–2024, 2014. 5
- [33] Muzaffer Özbey, Onat Dalmaz, Salman UH Dar, Hasan A Bedel, Şaban Öztürk, Alper Güngör, and Tolga Çukur. Un-supervised medical image translation with adversarial diffusion models. *IEEE TMI*, 2023. 2
- [34] Yongsheng Pan, Mingxia Liu, Chunfeng Lian, Tao Zhou, Yong Xia, and Dinggang Shen. Synthesizing missing pet from mri with cycle-consistent generative adversarial networks for alzheimer’s disease diagnosis. In *MICCAI*, pages 455–463, 2018. 2
- [35] Cheng Peng, Haofu Liao, Gina Wong, Jiebo Luo, S Kevin Zhou, and Rama Chellappa. Xraysyn: realistic view synthesis from a single radiograph through ct priors. In *AAAI*, pages 436–444, 2021. 1
- [36] Donald B Plewes and Walter Kucharczyk. Physics of mri: a primer. *Journal of Magnetic Resonance Imaging*, 35(5): 1038–1054, 2012. 9
- [37] Ali Razavi, Aaron Van den Oord, and Oriol Vinyals. Generating diverse high-fidelity images with vq-vae-2. *NeurIPS*, 32, 2019. 3
- [38] Robin Rombach, Andreas Blattmann, Dominik Lorenz, Patrick Esser, and Björn Ommer. High-resolution image synthesis with latent diffusion models. In *CVPR*, pages 10684–10695, 2022. 3
- [39] Anmol Sharma and Ghassan Hamarneh. Missing mri pulse sequence synthesis using multi-modal generative adversarial network. *IEEE TMI*, 39(4):1170–1183, 2019. 2, 5, 7
- [40] Haotian Tang, Yecheng Wu, Shang Yang, Enze Xie, Junsong Chen, Junyu Chen, Zhuoyang Zhang, Han Cai, Yao Lu, and Song Han. Hart: Efficient visual generation with hybrid autoregressive transformer. *arXiv preprint arXiv:2410.10812*, 2024. 3
- [41] Keyu Tian, Yi Jiang, Zehuan Yuan, Bingyue Peng, and Liwei Wang. Visual autoregressive modeling: Scalable image generation via next-scale prediction. *arXiv preprint arXiv:2404.02905*, 2024. 3
- [42] Michal R Tomaszewski and Robert J Gillies. The biological meaning of radiomic features. *Radiology*, 298(3):505–516, 2021. 9
- [43] Aaron Van Den Oord, Oriol Vinyals, et al. Neural discrete representation learning. *NeurIPS*, 30, 2017. 3, 4
- [44] Bao Wang, Yongsheng Pan, Shangchen Xu, Yi Zhang, Yang Ming, Ligang Chen, Xuejun Liu, Chengwei Wang, Yingchao Liu, and Yong Xia. Quantitative cerebral blood volume image synthesis from standard mri using image-to-image translation for brain tumors. *Radiology*, 308(2):e222471, 2023. 1, 2
- [45] Will Williams, Sam Ringer, Tom Ash, David MacLeod, Jamie Dougherty, and John Hughes. Hierarchical quantized autoencoders. *NeurIPS*, 33:4524–4535, 2020. 3
- [46] Yicheng Wu, Xiangde Luo, Zhe Xu, Xiaoqing Guo, Lie Ju, Zongyuan Ge, Wenjun Liao, and Jianfei Cai. Diversified and personalized multi-rater medical image segmentation. In *CVPR*, pages 11470–11479, 2024. 2
- [47] Jiahui Yu, Xin Li, Jing Yu Koh, Han Zhang, Ruoming Pang, James Qin, Alexander Ku, Yuanzhong Xu, Jason Baldridge, and Yonghui Wu. Vector-quantized image modeling with improved vqgan. In *ICLR*, 2022. 4
- [48] Lijun Yu, Yong Cheng, Kihyuk Sohn, José Lezama, Han Zhang, Huiwen Chang, Alexander G Hauptmann, Ming-Hsuan Yang, Yuan Hao, Irfan Essa, et al. Magvit: Masked generative video transformer. In *CVPR*, pages 10459–10469, 2023. 3
- [49] Qihang Yu, Mark Weber, Xueqing Deng, Xiaohui Shen, Daniel Cremers, and Liang-Chieh Chen. An image is worth 32 tokens for reconstruction and generation. *arXiv preprint arXiv:2406.07550*, 2024. 3
- [50] Wenyin Zhang, Yong Wu, Bo Yang, Shunbo Hu, Liang Wu, and Sahraoui Dhelim. Overview of multi-modal brain tumor mr image segmentation. In *Healthcare*, page 1051, 2021. 8
- [51] Yue Zhang, Chengtao Peng, Qiuli Wang, Dan Song, Kaiyan Li, and S Kevin Zhou. Unified multi-modal image synthesis for missing modality imputation. *IEEE TMI*, 2024. 2, 5
- [52] Chuanxia Zheng and Andrea Vedaldi. Online clustered codebook. In *ICCV*, pages 22798–22807, 2023. 4, 6
- [53] Chuanxia Zheng, Tung-Long Vuong, Jianfei Cai, and Dinh Phung. Movq: Modulating quantized vectors for high-fidelity image generation. *NeurIPS*, 35:23412–23425, 2022. 3